Inorg. Chem. **2007**, *46*, 9609–9615

A 3D Porous Cobalt–Organic Framework Exhibiting Spin-Canted Antiferromagnetism and Field-Induced Spin-Flop Transition

You-Gui Huang,[†] Da-Qiang Yuan,[†] Long Pan,[‡] Fei-Long Jiang,[†] Ming-Yan Wu,[†] Xu-Dong Zhang,[†] Wei Wei,[†] Qiang Gao,[†] Jeong Yong Lee,[‡] Jing Li,*[,‡] and Mao-Chun Hong*[,†]

State Key Laboratory of Structural Chemistry, Fujian Institute of Research on the Structure of Matter, Chinese Academy of Sciences, Graduate School of the Chinese Academy of Sciences, Fujian, Fuzhou, 350002, China, and Department of Chemistry and Chemical Biology, Rutgers University, 610 Taylor Road, Piscataway, New Jersey 08854

Received March 23, 2007

Two 3D cobalt–organic frameworks formulated as $[Co_3(2,4\text{-pydc})_2(\mu_3\text{-OH})_2]_n\cdot 5nH_2O$ (**1**) and $[Co_3(2,4\text{-pydc})_2(\mu_3\text{-OH})_2(H_2O)]_n\cdot 7nH_2O$ (**2**) (2,4-pydc = pyridine-2,4-dicarboxylate) have been hydrothermally synthesized and characterized. Both compounds **1** and **2** exhibit the 3D porous frameworks with hydroxyl-bridged metal Δ-chains. However, in comparison with only two crystallographically independent Co^{II} ions in a unit of **2**, three crystallographically independent Co^{II} ions are found in an asymmetric unit of **1**, where their Δ-chains are constructed by two types of vertexes sharing quadrangles formed via edge-sharing triangles. Magnetic studies show that **1** exhibits spin-canted antiferomagnetism and a field-induced spin-flop transition while **2** behaves as a normal antiferromagnet. The magnetic properties are largely retained by the porous frameworks of dehydrated **1** and **2** compounds. Gas adsorption measurements indicate that both the dehydrated compounds absorb H_2 into their pores.

Introduction

Multifunctional magnetic materials have caught increasing attention recently due to the possibility of producing materials where the magnetism can be modified by tuning the other.[1−5] Crystal engineering provides a powerful tool for the design and synthesis of magnetic materials with other functionalities.[2−5] Several research groups have reported some significant results in this context. In the past few years, Kobayashi et al. reported a number of molecule-based solids which combine electrical conductivity with magnetism.[3] Most of these solid materials are usually made by combining a conducting organic network with an inorganic magnetic component. Optical, magnetic materials have also been obtained by several groups.[4a−e] For these optical magnets, optical activity can be used to observe the switching of spin

* To whom correspondence should be addressed. E-mail: mchong@fjirsm.ac.cn (M.-C.H.); jlingli@rutchem.rutgers.edu (J.L.).
[†] Chinese Academy of Sciences.
[‡] Rutgers University.

(1) Humphrey, S. M.; Chang, J.-S.; Jhung, S. H.; Yoon, J. W.; Wood, P. T. *Angew. Chem., Int. Ed.* **2007**, *46*, 272.
(2) (a) Coronado, E.; Galán-Máscarós, J. R.; Gómez-García, C. J.; Laukhin, V. *Nature* **2000**, *408*, 447. (b) Alberola, A.; Coronado, E.; Galán-Máscarós, J. R.; Giménez-Saiz, C.; Gómez-García, C. J. *J. Am. Chem. Soc.* **2003**, *125*, 10774. (c) Clément, R.; Decurtins, S.; Gruselle, M.; Train, C. *Monatsh. Chem.* **2003**, *134*, 117. (d) Kurmoo, M.; Graham, A. W.; Day, P.; Coles, S. J.; Hursthouse, M. B.; Caulfield, J. L.; Singleton, J.; Pratt, F. L.; Hayes, W.; Ducasse, L.; Guioneeau, P. *J. Am. Chem. Soc.* **1995**, *117*, 12209.
(3) (a) Tanaka, H.; Kobayashi, H.; Kobayashi, A.; Cassoux, P. *Adv. Mater.* **2000**, *12*, 1685. (b) Fujiwara, E.; Fujiwara, H.; Kobayashi, H.; Otsuka, T.; Kobayashi, A. *Adv. Mater.* **2000**, *14*, 1376. (c) Fujiwara, H.; Kobayashi, H.; Fujuwara, E.; Kobayashi, A. *J. Am. Chem. Soc.* **2002**, *124*, 6816. (d) Zhang, B.; Tanaka, H.; Fujiwara, H.; Kobayashi, H.; Fujiwara, E.; Kobayashi, A. *J. Am. Chem. Soc.* **2002**, *124*, 9982. (e) Uji, S.; Shinagawa, H.; Terashima, T.; Yakabe, T.; Terai, Y.; Tokumoto, M.; Kobayashi, A.; Tanaka, H.; Kobayashi, H. *Nature* **2001**, *410* 908.
(4) (a) Sato, O. *Acc. Chem. Res.* **2003**, *36*, 692. (b) Sunatski, T.; Ikuta, Y.; Matsumoto, N.; Ohta, H.; Kojima, M.; Iijima, S.; Hayami, S.; Maeda, Y.; Kaizaki, S.; Dahan, F.; Tuchagues, J. P. *Angew. Chem., Int. Ed.* **2003**, *42*, 1614. (c) Lacroix, P. G.; Malafant, I.; Bénard, S.; Yu, P.; Rivière, E.; Nakatani, K. *Chem. Mater.* **2001** *13* 441. (d) Barron, L. D.; Buckingham, A. D. *Acc. Chem. Res.* **2001**, *34*, 781. (e) Inoue, K.; Kikuchi, K.; Ohba, M.; Ōkawa, H. *Angew. Chem., Int. Ed.* **2003**, *42*, 4810. (f) Gao, E. Q.; Yue, Y. F.; Bai, S. Q.; He, Z.; Yan, C. H. *J. Am. Chem. Soc.* **2004**, *126*, 1419. (g) Huang, Y. X.; Ewald, B.; Schnelle, W.; Prots, Y.; Kniep, R. *Inorg. Chem.* **2006**, *45* 7578. (h) Zeng, M. H.; Wang, B.; Wang, X. Y.; Zhang, W. X.; Chen, X. M.; Gao, S. *Inorg. Chem.* **2006**, *45* 7069. (i) Sato, O.; Kawakami, T.; Kimura, M.; Hishiya, S.; Kubo, S.; Einaga, Y. *J. Am. Chem. Soc.* **2004**, *126*, 13176.
(5) (a) Rujiwatra, A.; Kepert, C. J.; Claridge, J. B.; Rosseinsky, M. J.; Kumagai, H.; Kurmoo, M. *J. Am. Chem. Soc.* **2001**, *123*, 10584. (b) Kurmoo, M.; Kumagai, H.; Hughes, S. M.; Kepert, C. J. *Inorg. Chem.* **2003**, *42* 6709. (c) Wang, Z. M.; Zhang, B.; Kurmoo, M.; Green, A.; Fujiwara, H.; Otsuka, T.; Kobayshi, H. *Inorg. Chem.* **2005**, *44* 1230. (d) Beauvais, L. G.; Long, J. R. *J. Am. Chem. Soc.* **2002**, *124*, 12096. (e) Atwood, J. L. *Nat. Mater.* **2002**, *1*, 91.

10.1021/ic700559z CCC: $37.00
Published on Web 10/04/2007

states. In addition, chiral and switching (magnetism induced by light, pressure, adsorption of molecules, etc.) magnets have gained considerable attention because of their intriguing potential applications in enantioselective synthesis, asymmetric catalysis, and magnetic materials.[4f−i] Currently, an extended interest in this context is the design of molecular systems combining magnetism with porosity.[5] Particularly, porous magnets displaying magnetic hysteresis are of great importance because of the search for new and more efficient magnetic recording materials.[6] Unfortunately, the design of porous magnets is still a challenge since long-range magnetic ordering and porosity are inimical to one another.[7] One of the solutions to this antagonism is to link 0D clusters or 1D M−O−M inorganic chains by using the polycarboxylate ligands to form a 3D robust framework.[6c,8,9] Realizing this strategy, we selected pyridine-2,4-dicarboxylate acid which has been proven to be effective as spacers in porous frameworks.[1]

Herein, we report the syntheses, crystal structures, magnetic, and sorptive properties of two 3D porous cobalt−organic frameworks $[Co_3(2,4\text{-pydc})_2(\mu_3\text{-}OH)_2]_n\cdot 5nH_2O$ (**1**) and $[Co_3(2,4\text{-pydc})_2(\mu_3\text{-}OH)_2(H_2O)]_n\cdot 7nH_2O$ (**2**) (2,4-pydc = pyridine-2,4-dicarboxylate). A detailed comparison of the above two closely related phases demonstrates the subtle but important influence of the cobalt ion arrangements in the metal chains on the cooperative magnetism. Compound **1** crystallizing in a low-symmetry space group $P\bar{1}$ exhibits spin-canted antiferromagnetism and field-induced spin-flop transition, while **2** behaves as a normal antiferromagnet. Both dehydrated **1** and **2** compounds absorb H_2 into their pores.

Experimental Section

Materials and Methods. All of the chemicals were purchased from commercial suppliers and were used without further purification. Elemental analyses were carried out by the Elemental Analysis Lab of our Institute. The IR spectra were recorded as KBr pellets on a Spectrum One FT-IR spectrometer (Perkin-Elmer Instruments). X-ray powder diffraction data were recorded on a Rigaku MultiFlex diffractometer at 40 kV, 40 mA for Cu Kα (λ = 1.5406 Å) with a scan speed of 0.05−0.2 °/min. Simulated XRD patterns were calculated with the SHELXTL-XPOW program using the single-crystal data. TGA experiments were carried out at a heating rate of 10 °C/min in N_2 atmosphere. Magnetic measurements for powder samples of **1** and **2** were carried out with a Quantum Design PPMS model 6000 magnetometer. The H_2 adsorption/desorption measurements were performed at 77 K in the pressure range 0.001−1 atm using an Autosorb 1 MP (Quantachrome Instruments, Boynton Beach, FL). The sample was degassed for 5 h at 423 K. The total pore volume was calculated on the basis of the solvent-accessible volume estimated by the PLATON program.

Syntheses of Compounds 1 and 2. A mixture of cobalt powder (0.024 g, 0.4 mmol) and H_2pydc (0.032 g, 0.2mmol) was placed in a Teflon-lined Parr bomb containing 5 mL of deionized water and 0.5 mL of ethanol. The bomb was sealed, heated at 160 °C for 3 days, and allowed to cool to room temperature. After being filtered off, washed with water, and dried in air, a mixture of orange crystals of compound **1** (77 mg, yield 58%) and red crystals of **2** (27 mg, yield 20%) were obtained. The synthesis can be optimized to produce predominantly one compound or the other, so that a single-phase material is obtained following purification. For **1**, main IR absorption bands (cm^{-1}): 3439(s), 1629 (s), 1548(m), 1400(s), 1380(s), 1256(w), 1120(w), 1015(w), 730(w), 688(w). Anal. Calcd (%): C, 25.88; H, 3.08; N, 4.31. Found: C, 25.84; H, 3.06, N, 4.32. For **2**, main IR absorption bands (cm^{-1}): 3432(s), 1634(s), 1548(m), 1380(s), 1252(w), 824(w), 778(w) 726(m), 684(w). Anal. Calcd (%): C, 25.18; H, 3.30; N, 4.19. Found: C, 25.16; H, 3.28, N, 4.14. The phase purity of the bulk products was checked by comparing their observed and simulated XRD patterns (Figure S1).

Thermal Analyses. Preliminary thermogravimertric and differential thermal analyses for a crystalline sample of compound **1** in N_2 atmosphere showed three weight-loss steps. The first weight loss (17.6%) at 110 °C corresponds to the loss of H_2O occupied in the channels (calculated 16.7%). The second weight loss of 36% at 460 °C is attributed to decomposition of the framework. The third weight loss is 10.9% at 540 °C attributed to the formation of metal oxide. A TG analysis performed on a sample of **2** showed continuous weight loss (18.7%) between 30 and 120 °C, which corresponds to the loss of six water molecules per formula unit (calcd 18.9%). No further weight loss was observed until it reached 460 °C, at which point the decomposition of $[Co_3(2,4\text{-pydc})_2(\mu_3\text{-}OH)_2]_n$ occurred, as indicated by a significant weight loss (36.5%). The third weight loss is 10.8% at 540 °C, corresponding to the formation of metal oxide (Figure S2).

X-ray Crystallography. Several single crystals of compounds **1** and **2** were indexed on a SMART-CCD diffractometer with graphite-monochromated Mo Kα radiation (λ = 0.71073 Å). One crystal of each compound with good reflection quality was chosen for data collection. The structure was solved by direct methods and refined on F^2 by full-matrix least-squares using the SHELX97 program package.[10] The positions of H atoms were generated geometrically and allowed to ride on their parent carbon atoms. No attempt was made to locate the H atoms of lattice water molecules and hydroxyl ions. Details of the crystal data are summarized in Table 1. Selected bond lengths and bond angles of **1** and **2** are listed in Table 2. CCDC-603027 (**1**) and -603026 (**2**) contain supplementary crystallographic data for this paper.

Results and Discussion

Synthesis. The hydrothermal method has been extensively explored as an effective and powerful tool in the self-assembly of high-dimensional metal−organic coordination polymers, even though its reaction mechanism is still not clear.[11] As is known, many transition metal carboxylate compounds have been successfully obtained under hydrothermal conditions, which might be attributed to the poor

(6) (a) Xiang, S. C.; Wu, X. T.; Zhang, J. J.; Fu, R. B.; Hu, S. M.; Zhang, X. D. *J. Am. Chem. Soc.* **2005**, *127*, 16352. (b) Guillou, N.; Livage, C.; Drillon, M.; Férey, G. *Angew. Chem., Int. Ed.* **2003**, *42*, 5314. (c) Dietzel, P. D. C.; Morita, Y.; Blom, R.; Fjelvåg, H. *Angew. Chem., Int. Ed.* **2005**, *44*, 6354.
(7) (a) Férey, G. *Nat. Mater.* **2002**, *1*, 91. (b) Wang, Z. M.; Zhang, B.; Fujiwara, H.; Kobayashi, H.; Kurmoo, M. *Chem. Commun*, **2004**, 416.
(8) Guillou, N.; Livage, C.; van Beek, W.; Noguès, M.; Férey, G. *Angew. Chem., Int. Ed.* **2003**, *42*, 643.
(9) Kurmoo, M.; Kumagai, H.; Hughes, S. M.; Kepert, J. K. *Inorg. Chem.* **2003**, *42* 6709.
(10) Sheldrick, G. M. *SHELXTL*, Version 5.1; Bruker Analytical X-ray Systems Inc.: Madison, WI, 1997.
(11) (a) Liao, Y. C.; Liao, F. L.; Chang, W. K.; Wang, S. L. *J. Am. Chem. Soc.* **2004**, *126*, 1320. (b) Wang, Y.; Yu, J. H.; Guo, M.; Xu, R. R. *Angew. Chem., Int. Ed.* **2003**, *42*, 4809. (c) Neeraj, S.; Natarajan, S.; Rao, C. N. R. *Chem. Commun.* **1999**, 165. (d) Ayyappan, P.; Evans, O. R.; Lin, W. B. *Inorg. Chem.* **2002**, *41* 3328. (e) Li, X. J.; Wang, X. Y.; Gao, S.; Cao, R. *Inorg. Chem.* **2006**, *45* 1508.

Table 1. Crystal Data Collection and Structural Refinement Parameters

compound	**1**	**2**
formula	$C_{14}H_{20}N_2O_{16}Co_3$	$C_{14}H_{22}N_2O_{17}Co_3$
fw	649.11	667.13
a(Å)	11.1389(7)	17.5151(5)
b(Å)	11.2652(7)	13.7564(2)
c(Å)	11.4139(7)	10.8123(4)
α(deg)	76.3800(10)	
β(deg)	66.3690(10)	105.532(2)
γ(deg)	78.9640(10)	
V(Å^3)	1267.65(14)	2510.03(12)
Z	2	4
cryst syst	triclinic	monoclinic
space group	$P\bar{1}$	$C2/c$
cryst size(mm^3)	0.36 × 0.26 × 0.08	0.20 × 0.16 × 0.16
λ(Å)	0.71073	0.71073
ρ(g/cm^3)	1.701	1.765
μ(mm^{-1})	2.014	2.039
T(K)	273(2)	273(2)
total reflns	6650	3515
unique data collected	4440	2195
observed reflns	3943	1927
R_{int}	0.0303	0.0403
data/restraints/params	4440/335/12	2195/0 /177
$R^a(I > 2\sigma(I))$	0.0762	0.0816
$R_w{}^a(I > 2\sigma(I))$	0.0.1930	0.1822
R^a(all data)	0.0866	0.0962
$R_w{}^a$(all data)	0.2066	0.1914
GOF	1.044	1.178

[a] $R = \sum||F_o| - |F_c||/\sum|F_o|$, $R_w = [\sum w(F_o^2 - F_o^2)^2/\sum w(F_o^2)^2]^{1/2}$.

solubility of carboxylate ligands.[12] In this article, orange crystals of compound **1** and red crystals of **2** were also isolated from the hydrothermal reaction of cobalt powder and H_2pydc. Obviously, the Co(II) ions found in **1** and **2** were created through the oxidation of Co(0) starting material under hydrothermal conditions. The synthesis can be optimized to produce predominantly one compound or the other, so that single-phase material is obtained following purification. It should be mentioned that during the course of our investigation for **1** and **2**, Wood et al. have also obtained compound **2** by employing a Co(II) starting material, $CoCl_2 \cdot 6H_2O$, as a cobalt precursor to react with H_2pydc in alkaline media.[1]

Structural Description. The X-ray diffraction analyses of **1** and **2** show them to have simple and closely related formulas but show the extremely complex and entirely different structures. The crystal structure of **2** exhibits a 3D porous framework with hydroxyl-bridged metal chains where the Δ-chains are constructed by one type of triangles sharing the edges and vertexes (Figure 1).[1] As above in **2**, compound **1** is also built on a 3D porous framework consisting of strips of corner- and edge-sharing $Co_3(\mu_3$-OH) triangles. In comparison with only two crystallographically independent Co(II) ions in the asymmetric unit of **2**, three crystallographically distinct Co sites are found in **1**. Co1 adopts an octahedral coordination geometry in which two μ_3-OH oxygen atoms stand at the apical positions and four carboxylate oxygen atoms comprise the equatorial plane. Co3 is also pseudo-octahedrally coordinated to an oxygen only donor set, comprised of trans coordination by the carboxylate O and H_2O and equatorial cis coordination of carboxylate-O and μ_3-OH oxygen (O9 and O10) atoms. While Co2 is in a greatly distorted octahedral geometry by two N atoms and two O atoms from two chelated 2,4-pydc ligands and two μ_3-OH groups (Figure 2). Co1 and Co2 are connected via O9 hydroxide group, resulting in a $Co_3(\mu_3$-OH) triangle, and two triangles share a common edge, forming a tetrameric

Table 2. Selected Bond Lengths (Å) and Angles (deg) for **1** and **2**[a]

Compound **1** (bond)			
Co1−O10	2.012 (4)	Co2−O9^{iii}	2.105 (4)
Co1−O6^{i}	2.062 (5)	Co2−N2	2.125 (6)
Co1−O9	2.093 (4)	Co2−N1	2.129 (6)
Co1−O4^{ii}	2.099 (5)	Co3−O10^{iv}	2.058 (5)
Co1−O1^{iii}	2.122 (5)	Co3−O5^{v}	2.072 (5)
Co1−O8	2.179 (5)	Co3−O10	2.093 (4)
Co2−O9	2.071 (5)	Co3−O7	2.124 (5)
Co2−O1	2.072 (5)	Co3−O3^{vi}	2.130 (5)
Co2−O8	2.100 (5)	Co3−O11	2.180 (6)
Compound **1** (angle)			
O10−Co1−O6^{i}	101.1 (2)	O1−Co2−N1	76.6 (2)
O10−Co1−O9	164.03 (18)	O8−Co2−N1	105.4 (2)
O6^{i}−Co1−O9	92.4 (2)	O9^{iii}−Co2−N1	156.4 (2)
O10−Co1−O4^{ii}	93.5 (2)	N2−Co2−N1	93.1 (2)
O6^{i}−Co1−O4^{ii}	87.3 (2)	O10^{iv}−Co3−O5^{v}	98.2 (2)
O9−Co1−O4^{ii}	95.77 (19)	O10^{iv}−Co3−O10	81.10 (18)
O10−Co1−O1^{iii}	91.35 (19)	O5^{v}−Co3−O10	176.6 (2)
O6^{i}−Co1−O1^{iii}	93.0 (2)	O10^{iv}−Co3−O7	171.64 (18)
O9−Co1−O1^{iii}	79.26 (18)	O5^{v}−Co3−O7	87.3 (2)
O4^{ii}−Co1−O1^{iii}	175.03 (19)	O10−Co3−O7	93.78 (18)
O10−Co1−O8	89.32 (18)	O10^{iv}−Co3−O3^{vi}	97.64 (19)
O6^{i}−Co1−O8	169.3 (2)	O5^{v}−Co3−O3^{vi}	87.5 (2)
O9−Co1−O8	77.74 (18)	O10−Co3−O3^{vi}	89.3 (2)
O4^{ii}−Co1−O8	89.7 (2)	O7−Co3−O3^{vi}	88.9 (2)
O1^{iii}−Co1−O8	89.1 (2)	O10^{iv}−Co3−O11	90.0 (2)
O9−Co2−O1	99.9 (2)	O5^{v}−Co3−O11	85.9 (2)
O9−Co2−O8	80.02 (18)	O10−Co3−O11	97.4 (2)
O1−Co2−O8	178.0 (2)	O7−Co3−O11	84.1 (2)
O9−Co2−O9^{iii}	85.43 (17)	O3^{vi}−Co3−O11	170.6 (2)
O1−Co2−O9^{iii}	80.09 (19)	O1−Co2−N1	76.6 (2)
O8−Co2−O9^{iii}	97.94 (19)	Co2−O9−Co1	103.0 (2)
O9−Co2−N2	155.8 (2)	Co2−O9−Co2^{iii}	94.57 (17)
O1−Co2−N2	104.1 (2)	Co1−O9−Co2^{iii}	100.18 (19)
O8−Co2−N2	75.9 (2)	Co1−O10−Co3^{iv}	111.8 (2)
O9^{iii}−Co2−N2	95.9 (2)	Co1−O10−Co3	122.6 (2)
O9−Co2−N1	95.1 (2)	Co3^{iv}−O10−Co3	98.90 (18)
Compound **2** (bond)			
Co1−O3^{i}	2.067 (6)	Co2−O5^{v}	2.107 (6)
Co1−O5	2.085 (5)	Co2−O1	2.109 (6)
Co1−O1	2.105 (6)	Co2−N1	2.141 (7)
Co2−O2^{iv}	2.072 (6)	Co2−O4^{ii}	2.167 (7)
Co2−O5	2.096 (5)		
Compound **2** (angle)			
O3^{i}−Co1−O3^{ii}	85.0 (4)	O5−Co2−O1	77.3 (2)
O3^{i}−Co1−O5	90.8 (2)	O5^{v}−Co2−O1	95.4 (2)
O3^{i}−Co1−O5^{iii}	95.7 (2)	O2^{iv}−Co2−N1	93.8 (3)
O5−Co1−O5^{iii}	171.1 (3)	O5−Co2−N1	151.4 (3)
O3^{i}−Co1−O1	168.3 (2)	O5^{v}−Co2−N1	90.0 (2)
O3^{ii}−Co1−O1	93.8 (2)	O1−Co2−N1	76.2 (2)
O5−Co1−O1	77.7 (2)	O2^{iv}−Co2−O4^{ii}	77.5 (3)
O5^{iii}−Co1−O1	96.0 (2)	O5−Co2−O4^{ii}	95.9 (2)
O1−Co1−O1^{iii}	89.6 (3)	O5^{v}−Co2−O4^{ii}	177.6 (3)
O2^{iv}−Co2−O5	114.7 (3)	O1−Co2−O4^{ii}	85.0 (3)
O2^{iv}−Co2−O5^{v}	102.5 (2)	N1−Co2−O4^{ii}	92.4 (3)
O5−Co2−O5^{v}	81.9 (2)	Co1−O5−Co2	97.5 (2)
O2^{iv}−Co2−O1	159.5 (3)	Co1−O5−Co2^{v}	120.6 (3)

[a] Symmetry codes: (i) x, $1 + y$, z; (ii) $-x$, $1 - y$, $1 - z$; (iii) $-1 - x$, $1 - y$, $1 - z$; (iv) $-1 - x$, $1 - y$, $2 - z$. for **1**; (i) $-1/2 + x$, $-1/2 + y$, z; (ii) $1/2 - x$, $-1/2 + y$, $1/2 - z$; (iii) $-x$, y, $1/2 - z$; (iv) x, $2 - y$, $-1/2 + z$; (v) $-x$, $2 - y$, $-z$ for **2**.

(12) (a) Wang, X. L.; Qin, C.; Wang, E. B.; Xu, L.; Su, Z. M.; Hu, C. W. *Angew. Chem., Int. Ed.* **2004**, *43*, 5036. (b) Liu, Y. H.; Ku, Y. L.; Wu, H. C.; Wang, J. C.; Lu, K. L. *Inorg. Chem.* **2002**, *41* 2592. (c) Shi, Z.; Li, G. H.; Wang, L.; Gao, L.; Chen, X. B.; Hua, J.; Feng, S. H. *Cryst. Growth Des.* **2004**, *4*, 25.

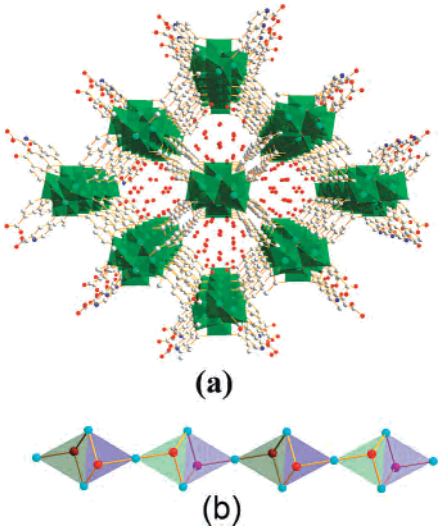

Figure 1. Crystal structures of **2** showing 3D porous framework (a) with hydroxyl-bridged metal chains (b).

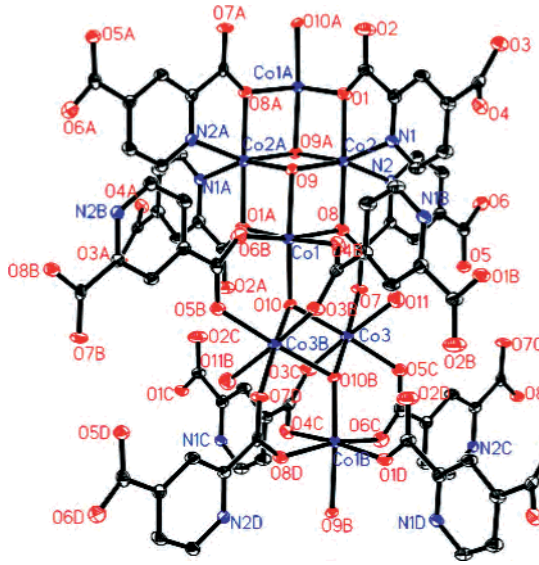

Figure 2. Crystal structures of **1** showing complete coordination environments of cobalts environments. All hydrogen atoms are omitted for clarity. The symmetry codes are A: $-x-1, 1-y, 1-z$; B: $-x-1, 1-y, 2-z$; C: $x, 1+y, z$; and D: $x-1, y, 1+z$.

unit. Co1 is also connected with Co3 via the O10 hydroxide group to give another $Co_3(\mu_3\text{-OH})$ triangle which shows greater distortion than that formed via Co1 and Co2. Two triangles also share an edge, forming a different tetrameric unit. Therefore, two distinct tetrameric units are present in **1**, which differ from compound **2**. The two distinct tetrameric units are arranged alternately sharing vertexes, resulting in a chain with the Δ-chain topology (Figure 3a). Interestly, Co1 and Co2 are further bridged via μ_2-O1 and μ_2-O8, forming an incomplete face-sharing double cube. Co1 is also linked to Co3 by three carboxylate moieties, resulting in a beautiful face-sharing double basket. The incomplete double cubes and the double baskets are arranged to alternately share edges to furnish an inorganic chain (Figure 3b). Furthermore, similar to compound **1**, each inorganic chain in **1** connects to four orthogonal adjacent chains forming a 3D open framework with 1D solvent-filled channels (Figure 4).

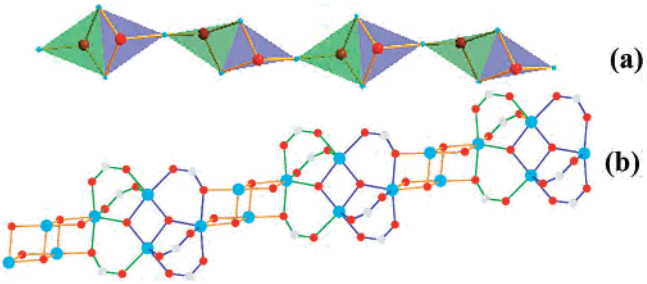

Figure 3. (a) Inorganic chain composed of vertex-sharing tetrameric units formed by edge-sharing triangles in **1**. (b) Chain of incomplete face-sharing double cubes and double flower baskets in **1**.

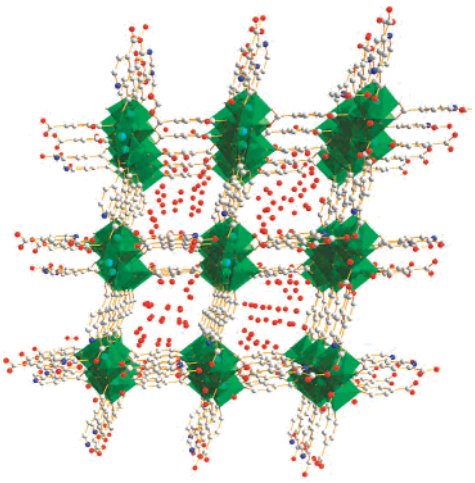

Figure 4. Polyhedron view of the 3D open framework of **1** with 1D solvent-filled channels.

Magnetic Properties. Compound 1. The magnetic susceptibility data of **1** per Co_3 unit under 10 kOe external field in the temperature range 50−300 K obeys the Curie−Weiss law, giving $\theta = -78$ K, thus indicating a dominant strong antiferromagnetic interaction and/or spin orbital coupling between the Co^{II} ions (Figure 5a). Although the Δ-chain topology has been observed a number of times in cobalt compounds with the stoichiometry $Co_3(L)_2(\mu_3\text{-OH})_2$ (whele L is a dianionic ligand),[1,14b,21] there is still no appropriate theoretical model to estimate the magnetic exchange between adjacent Co(II) ions in this complicated system. The μ_{eff} value decreases to a minimum and then increases slightly to reach

(13) Gutschke, S. O. H.; Price, D. J.; Powell, A. K.; Wood, P. T. *Angew. Chem., Int. Ed.* **1999**, *38*, 1088.
(14) (a) Colacio, E.; Domínguez-Vera, J. M.; Ghazi, M.; Kivekäs, R.; Lloret, F. J.; Moreno, M.; Stoeckli-evans, H. *Chem. Commun*, **1999**, 987. (b) Humphrey, S. M.; Wood, P. T. *J. Am. Chem. Soc.* **2004**, *126*, 13236.
(15) Mydosh, J. A. *Spin Glasses: An Experimental Introduction*; Taylor and Francis: London. 1993.
(16) Zheng, Y. Z.; Tong, M. L.; Zhang, W. X.; Chen, X. M. *Angew. Chem., Int. Ed.* **2006**, *45*, 6310.
(17) Yoon, J. H.; Lim, J. H.; Choi, S. W.; Kim, H. C.; Hong, C. S. *Inorg. Chem.* **2007**, *46* 1529.
(18) Zheng, L. M.; Gao, S.; Yin, P.; Xin, X. Q. *Inorg. Chem.* **2004**, *43* 2151.
(19) (a) Dzyaloshinsky, L. *Phys. Chem. Solids* **1958**, *4*, 421. (b) Moriya, T. *Phys. Rev.* **1960**, *120*, 91. (c) Armentano, D.; Munno, G. D.; Lloret, F.; Palli, A.; Julve, V. M. *Inorg. Chem.* **2002**, *41* 2007.
(20) Spek, L. *A Multipurpose Crystallographic Tool*; Utrecht University: Utrecht, Netherlands, 1999.
(21) (a) Gutschke, S. O. H.; Molinier, M.; Powell, A. K.; Wood, P. T. *Angew. Chem., Int. Ed.* **1997**, *36*, 991. (b) Gerrard, L. A.; Wood, P. T. *Chem. Commun*, **2000**, 1670.

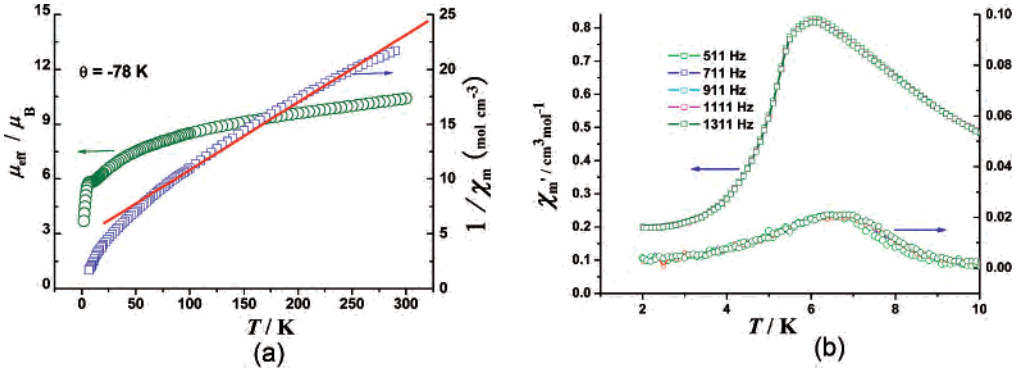

Figure 5. (a) Temperature dependence of μ_{eff} and $1/\chi_m$ for **1** at 10 KOe. (b) Temperature dependence of ac χ_m at different frequencies for **1**. ($H_{dc} = 0$ Oe, $H_{ac} = 3$ Oe)

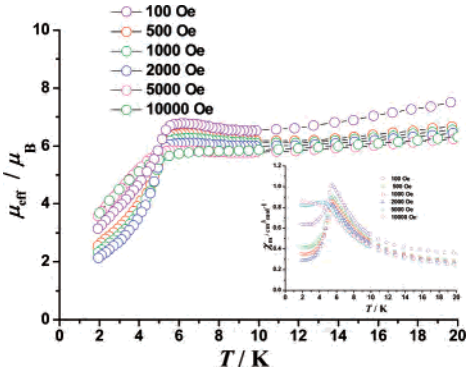

Figure 6. Plots of temperature dependence of μ_{eff} at different fields for **1**. The inset is the plots of temperature dependence of χ_m at different fields for **1**.

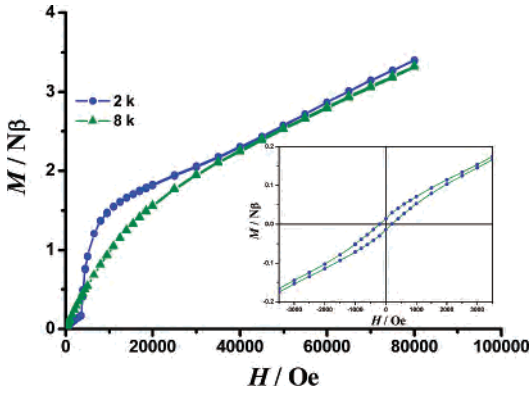

Figure 7. Plots of M vs H at 2 and 8 K for **1**. The inset shows hysteresis loop at 2 K.

a maximum at about 6 K and finally decreases more rapidly on further cooling (Figure 6). This behavior is characteristic of canted antiferromagnetism[13] in which a predominantly antiferromagnetic phase possesses a small spontaneous magnetization due to a small deviation from a strictly antiparallel arrangement. A series of temperature scans in various fields show field dependence of the low-temperature phase confirming our assignment. In small fields below 6 K, the susceptibility increases as the measuring field decreases, consistent with canted antiferromagnetism.[14b] At low field and below 3.0 K, a slow rise in χ_m pertains to the occurrence of spin-canting (Figure 6 inset).[14] On the other hand, the broad peak appearing around 6 K in the χ_m vs T curve is typical for a low-dimensional antiferromagnet.[18] Considering that the Δ-chains are well isolated by pydc spacers (the shortest Co···Co distance between the chains is 9.01 Å), a low-dimensional magnet is anticipated. When the strength of external field exceeds 5000 Oe, the peak disappears, suggesting the occurrence of a field-induced spin-flop transition[22] (Figure 6 inset). Evidence for the spin-canting and spin-flop transition was further confirmed by the ac susceptibility measurements.

To further inspect the underlying magnetic nature, the measurements of ac magnetic susceptibility were carried out at zero dc field. The real part (χ_m') of ac susceptibility shows that a maximum is detectable at 6 K. The observation of a peak in χ_m'' at about 6 K is relevant with magnetized state, thus indicating that a partly canted antiferromagnetic structure exists (Figure 5b). In addition, no obvious frequency-dependent behavior is observed in **1**, which precludes the possibilities of a spin-glass or SCM (single chain magnet).[15−16] It is known that the real part (χ_m') of ac susceptibility below T_N varies according to the following expression:[23]

$$\chi = \chi_0(1 - T/T_N)^{-\gamma} \quad (1)$$

where γ is the critical exponent and χ_0 is the critical amplitude below T_N. The value γ provides information about the dimensionality and the symmetry of the magnetic lattice undergoing the ordering transition.[22−23] Figure S4 shows the double logarithmic plot of χ_m' as a function of the reduced temperature. A fitting of the data to eq 1 yielded $\gamma = 0.80$. The obtained critical exponent is smaller than the values experimentally found in 3D ferromagnets[23a] ($\gamma \approx 1.3$). However, it is close to the values found for spin-flop transition[23d] ($\gamma \approx 0.56$) and canted system[23e] ($\gamma \approx 0.35-0.7$).

The field dependence of the magnetization (M) in the field range from −8 to +8 T is shown in Figure 7. The magnetization curve at 2 K shows a two-step transition. At

(22) Feng, M. L.; Prosvirin, A. V.; Mao, J. G.; Dunbar, K. R. *Chem. Eur. J.* **2006**, *12*, 8312.

(23) (a) Binney, B. B.; Dowrick, N. J.; Fisher, A. J.; Newman, M. E. J.; *The theory of critical phenomena*; Clarendon: Oxford, 1992. (b) Girtu, M. A.; Wynn, C. M.; Zhang, J.; Miller, J. S.; Epstein, A. J. *Phys. Rev. B* **2000**, *61*, 492. (c) Belayachi, A.; Dormann, J. L.; Nogues, M. *J. Phys. Condens. Matter* **1998**. *10*, 1599. (d) Kawamura, H.; Caille, A.; Plumer, M. L. *Phys. Rev. B* **1990**, *41*, 4416. (e) Dormann, J. L.; Belayachi, A.; Nogues, N. *J. Magn. Magn. Mater.* **1992**, *104*, 239.

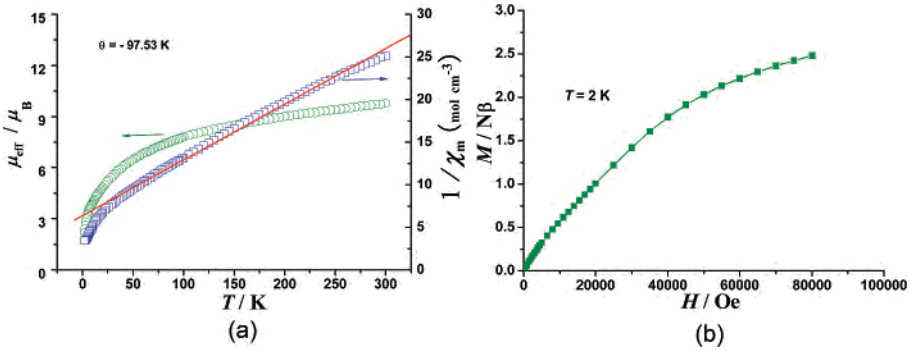

Figure 8. (a)Temperature dependence of μ_{eff} and $1/\chi_m$ for **2**. (b) Field dependence of magnetization of **2** at 2 K.

low field below 800 Oe, there is a relatively rapid increase of *M*. Above 800 Oe, a sigmoid-shaped curve is found; the magnetization increases very slowly between 800 and 5000 Oe due to strong antiferromagnetic interactions followed by a sharp increase. The magnetization then increases gradually to 80 KOe without saturation and exhibits a value (M = 3.5 $N\mu_B$) that is far from the theoretical three expected Co^{2+} ions ($M_s \approx 6.9N\ \mu_B$). Assuming the nearly linear increase of the magnetization, the expected saturation magnetic field (H_c) is about 211 KOe. The transition at about 800 Oe appears to be associated with spin-canting,[14,17] and the spin-flop field (H_{SF}) appears at about 5000 Oe determined by the d*M*/d*H* derivative curve (Figure S5). With theses results, the anisotropy field $H_A \approx 119$ Oe and the exchange field $H_E \approx$ 106 KOe. Furthermore, the magnetic hysteresis loop at 2 K with a coercive field 200 Oe, and remnant magnetization (*M*r) of 80 Oe emu mol^{-1} (Figure 7 inset) confirm the occurrence of spontaneous magnetization of **1**, in agreement with the observed spin-canting. Notably, these magnetic properties are largely retained by the porous network of dehydrated **1**. Like compound **1**, the μ_{eff} value for dehydrated **1** decreases to a minimum and then increases slightly to reach a maximum at about 5 K, and finally decreases on further cooling (Figure S7). This behavior is characteristic of spin-canted antiferromagnetism. The hysteresis in low field cooperative with a sigmoid-shaped curve above 800 Oe further confirms above spin-canted antiferromagnetism and field-induced spin-flop transition (Figure S6a).

Compound 2. For comparison, the magnetic property of compound **2** with a formula closely related to **1**, was studied. The temperature dependence of magnetic susceptibility χ_m for the powder sample of **2** is investigated in the range 2−300 K under 10 kOe applied field (Figure 8a) (χ_m is the magnetic susceptibility per Co_3 unit). A Curie−Weiss fit to the high-temperature susceptibility data yields a θ of −98 K, indicating that strong antiferromagnetic coupling dominates the exchange between Co ions within the chain. The single-ion behavior of octahedral Co(II) could also make partial contribution to the negative θ, but not to such a large value.[11e] As the temperature is lowered, the μ_{eff} value exhibits a monotonic decrease to 2.2 μ_B at 2 K, consistent with the simple antiferromagnetic behavior. Furthermore, the antiferromagnetic nature of the complex is further supported by the magnetization vs field curve measured at 2 K (Figure 8b). The $M-H$ curve shows a slow nearly linear increase with increasing field, and no detectable hysteresis was observed at very low fields, which is consistent the overall antiferromagnetic ordering. Remarkably, like compound **1**, the antiferromagnetic nature is largely retained by the porous framework of dehydrated **1** supported by its $M-H$ curve (Figure S6b).

Compared with compound **2**, a mechanism of ferromagnetic-like correlation exists in **1**, which can be attributed to spin-canting. It is well-known that spin-canting may arise from two mechanisms: single-ion magnetic anisotropy and antisymmetric exchange.[19] From a structural point of view, we believe that the spin-canting may be favored by the significant spin−orbit coupling associated with the $^4T_{1g}$ ground term of Co(II) ions and the three different coordination environments shown by the three Co(II) ions and is consistent with the crystallization of **1** in a low-symmetry space group $P\bar{1}$.

Porosity and Adsorption Phenomena. The openness of the channels makes them possible to remove the guest water molecules from compounds **1** and **2**. Evacuation of $[Co_3(2,4\text{-pydc})_2(\mu_3\text{-OH})_2]_n \cdot 5nH_2O$ and $[Co_3(2,4\text{-pydc})_2(\mu_3\text{-OH})_2(H_2O)]_n \cdot 7nH_2O$ at 150 °C removed the guest water molecules quantitatively, affording the dehydrated solid, whose XRD patterns are consistent with those of original materials. This indicates preservation of the framework and retention of the crystalline order upon removal of the guest species. Furthermore, according to TG analyses, both the frameworks retain stable up to 460 °C, at which point they begin to decompose.

The well-defined structures of the dehydrated frameworks allow us to estimate their pore window sizes and volume by computationally removing the guest water molecules. The space-filling models suggest that the aperture in **1** is of an approximately rhombus contour with a dimension (~9.01 Å) large enough for uptake of adsorbates (Figure S3a); while the aperture in **2** is of an approximately square contour with a dimension (~9.19 Å) (Figure S3b). As estimated by the PLATON program,[20] compounds **1** and **2** have the solvent-accessible volume accounting for 39.4% and 43.4%, respectively.

To experimentally evaluate the pore characteristics of two structures and to analyze their hydrogen-adsorption properties, as well as to understand the differences in their pore structures, we carried out an extensive gas-adsorption study at 77 K. The hydrogen adsorption−desorption isotherms for

1 and **2** at 77 K are plotted in Figure S8. Compound **1** adsorbs less hydrogen than compound **2**. At 1 atm, the values are 0.70 and 1.02 wt % for **1** and **2**, respectively. Another interesting feature of the isotherms is the hysteresis loop between the adsorption and desorption branches.

Conclusions

We have synthesized two porous cobalt−organic frameworks based on hydroxyl-bridged Δ-chain structures. The Δ-chains in **1** are constructed by two types of vertexes sharing quadrangles formed through edge-sharing triangles, while those in **1** are constructed by one type of triangles sharing edges and vertexes. Consistent with the structural diversity, the magnetic properties of these two compounds are also distinct from each other dramatically. Compound **1** exhibits unprecedented spin-canted antiferromagnetsim and field-induced spin-flop transition. Compound **2** represents a simple antiferromagnet. It is possible to remove the guest water molecules, while both **1** and **2** maintain their framework structures intact so that the magnetic properties are largely retained in their dehydrated state. The most striking feature of these porous frameworks is their sorption capability to hydrogen. This work demonstrates the importance of crystal engineering of coordination polymers in the field of multifunctional molecular-based magnetic materials.

Acknowledgment. This work was supported by the grants of the National Natural Science Foundation of China and the Natural Science Foundation of Fujian Province. We thank Miss J. Zhang and Dr. X. T. Wang for technical assistance and discussions.

Supporting Information Available: Crystallographic data in CIF format and various plots of data. This material is available free of charge via the Internet at http://pubs.acs.org.

IC700559Z